Electronic Supplementary Material (ESI) for Nanoscale.

Electronic Supplementary Information for

Quantifying the Force in Flow-Cell Based Single-Molecule Stretching Experiment

Jialun Liang, [a,b] Jiaxi Li, [a,b] Zhensheng Zhong, [a,b] Thitima Rujiralai, [c] Jie Ma*[a,b]

[a.] *School of Physics, Sun Yat-sen University, Guangzhou 510275, Guangdong, China.*

[b.] *State Key Laboratory of Optoelectronic Materials and Technologies, Sun Yat-sen University, Guangzhou 510275, Guangdong, China*

[c.] *Division of Physical Science, Faculty of Science, Prince of Songkla University, Hat Yai, Songkhla, 90112, Thailand*

** Corresponding author: majie6@mail.sysu.edu.cn*

1. Calibration of the relationship between pixel spacing and real-space distance in the imaging system

In the experiment, X and Y positions of the bead are measured in pixels. Therefore, they have to be converted to real-space dimensions for DNA extension measurement. Our imaging system is composed of a 40× oil immersion objective, a 1" tube lens (f = 200 mm), a mirror, and a CMOS camera which has a pixel size of 8 μm × 8 μm. Therefore, theoretically one pixel should correspond to 200 nm under this 40× magnification. In practice, to be certain about this conversion factor, we calibrate it by using a nano-fabricated "ruler"[1] as shown in Fig. S1A. This nano-ruler is a 40×40 nano-hole array with the distance between the adjacent nano-holes equal to 2 μm. For the image of one nano-hole, the 2D greyscale intensity distribution is shown in Fig. S1B. To find out the center of the nano-hole, the greyscale intensities from all rows (or all columns) for one nano-hole in a region of interest (ROI) of 8×8 pixels were firstly accumulated to get the x profile (or y profile). Then the x (or y) center of a nano-hole is determined by using a quadratic fit to the x profile (or y profile) as shown in Fig. S1C. As an example, the determined center positions (in pixel) of the 10×10 nano-holes chosen from the yellow rectangular region in Fig. S1A are plotted in Fig. S1D. Because the nano-hole array cannot be perfectly aligned with the $\hat{x}$ and $\hat{y}$ direction of the camera and there will be a small tilt angle θ. Given the row index i (i = 0 to 9) and column index j (j = 0 to 9) for the nano-hole array, the tilt angle θ_i related to the $\hat{x}$ direction of the camera can be extracted from the slope of the linear fitting of the center positions of nano-holes in the i^{th} row as shown in Fig. S1D. Consequently, the real-space distance along $\hat{x}$ between the j^{th} and the first nano-holes in the i^{th} row can be written as $x_{real,i,j} = 2j\cos\theta_i$ μm where "2" comes from the real-space distance between two adjacent nano-holes, *i.e.*, 2 μm. We plot the x coordinate in μm (x_{real}) of each nano-hole center in the i^{th} row versus its corresponding x coordinate in pixel (x_{pixel}) as shown in Fig. S1E, and then fit it with a straight line. The slope k_i from fitting thus represents the x conversion factor for the i^{th} row. In the end, we average all the k_i (for i = 0 to 9) to obtain the final x conversion factor. Similarly, we can also get the y conversion factor (see Fig. S1F). The final calibrated x and y conversion factors are 199.06 nm pixel^{-1} and 199.63 nm pixel^{-1}, respectively, which are very close to the

theoretically predicted value, *i.e.*, 200 nm pixel^{-1}. Therefore, in practice, we simply use the theoretical value, *i.e.*, 200 nm pixel^{-1}, to convert the measured pixels into real-space distance.

2. Image analysis algorithm for real-time bead tracking

The algorithm used for real-time bead tracking is similar to that previously reported in literatures.[2-5] In brief, when a typical image of a bead is obtained as shown in Fig. S2A, a rectangular ROI (usually 120 pixels × 120 pixels) surrounding the diffraction pattern of the bead is assigned. The greyscale intensity of the ROI is cross-correlated with its mirror function by using fast Fourier transform operations.[4] The results for x and y coordinates are shown in Fig. S2B and S2C, respectively. After that, the coordinates of the bead center, *i.e.*, x_{center} and y_{center}, are obtained by a 5-point quadratic fit to the data around the maximum in the cross-correlation signal (see the insets in Fig. S2B and S2C). Further, to obtain z position of the bead, a radial profile of the greyscale intensity of bead pattern is constructed in a polar coordinate in which the point (x_{center} , y_{center}) is set as the origin, as shown in Fig. S2D.[2-5] To correct for the fluctuations in the illumination light, the radial profile is normalized by subtracting its mean intensity and then dividing by the standard deviation of the intensity. To estimate the bead's z position, the radial profile of the bead is compared with a Look-Up-Table (LUT)[5] which is constructed at the beginning of the experiment by recording the bead's radial profiles when setting objective at different position z using a nano-piezo stage. Fig. S2E shows a typical process of building a LUT. The nano-piezo stage moves from z_0 to (z_0+4) μm at a step size of 100 nm, which causes the objective focal plane to move from the black dash line to the red, as shown in the cartoon in Fig. S2E. Notice here due to the focal-shift effect, the objective focal plane actually only moves 4ζ_{fs} μm. Here ζ_{fs} is the focal-shift and is given by the refractive index ratio of water and glass, *i.e.*, $\zeta_{\text{fs}} = n_{\text{water}}/n_{\text{glass}} \approx 0.88$. Meanwhile, the bead's radial profile changes from the deep green curve to the light green curve in Fig. S2E. During the experiment, the bead's radial profile (RP_{bead}) is compared with the LUT by calculating the squared differences (LUT diff) between RP_{bead} and all the radial profiles in LUT, as shown in Fig. S2F. The final z position of the bead is deduced via a ten-point quadratic fit to get the minimum (see the inset in Fig. S2F) followed by the multiplication of ζ_{fs}. For the flow-cell experiment, we select a stuck bead in the field of view to construct one LUT and

then apply this LUT to all tethered beads in the same view. The distance between the bottom of the tethered bead to the surface of cover-slip is obtained by subtracting the tethered bead's z position from the stuck bead's z position assuming that the size of these beads are equal.

3. Calculation of the velocity distribution of the flow

The Reynolds Numbers under our experimental conditions are small, typically less than 30. We thus refer to a symmetric solution for the velocity profile in a laminar flow proposed by Spiga *et al.*[6] to calculate the velocity distribution of the flow. Given the momentum Navier Stokes equation and the nonslip boundary conditions, Spiga *et al.* proposed a general solution for the dimensionless velocity $v^*(x, z)$ and the dimensionless average velocity w^* as

$$v^*(x,z) = \frac{16\beta^2}{\pi^4}\sum_{n\ \mathrm{odd}}^{\infty}\sum_{m\ \mathrm{odd}}^{\infty}\frac{\sin(n\pi\frac{x}{a})\sin(m\pi\frac{y}{b})}{nm(\beta^2 n^2 + m^2)} \tag{S1}$$

$$w^* = \frac{64}{\pi^6}\sum_{n\ \mathrm{odd}}^{\infty}\sum_{m\ \mathrm{odd}}^{\infty}\frac{1}{n^2 m^2(n^2 + \frac{m^2}{\beta^2})} \tag{S2}$$

where a is the width of the channel, b is the height of the channel and β is equal to b/a. The coordinate system is defined as Fig. S6A shows. Both v^* and w^* converge quickly with n and m. The calculated velocity is accurate enough when setting the maximum of n and m in eqn (S1) and (S2) as 100. The calculated velocity profile at z = 1 μm along $\hat{x}$ direction is shown in Fig. S6B and the velocity profile at x = 0.5a along $\hat{z}$ direction is shown in Fig. S6C. The relationship between v^* and z is quite linear when z is close to the surface as shown in Fig. S6D. Then, we can calculate the dimensional velocity $v(x, z)$ by eqn (S3) to (S5) with the volume flow rate, V, and the height z given from experiments.

$$w = \frac{V}{ab} \tag{S3}$$

$$k_v = \frac{w}{w^*} \tag{S4}$$

$$v(x, z) = k_v \, v^*(x, z) \tag{S5}$$

Here, w is the dimensional average velocity, and k_v is a proportional coefficient. Since the velocity profile is quite flat along $\hat{x}$ direction as Fig. S6B shows, the dimensionless velocity $v^*(x, z)$ at different x can be obtained by $v^*(x, z) \approx v^*(0.5a, z)$.

4. The "bead-spring chain" model for DNA hydrodynamic drag effect evaluation

4.1 The hydrodynamic drag effect on the force calibration using bead's Brownian motions

According to the Taylor expansion of E_p around the equilibrium position $\vec{r}_0 = (0, y_0, z_0)$,[7]

$$E_\mathrm{p}(\vec{r}) \approx E_\mathrm{p}(\vec{r}_0) + \frac{1}{2}\frac{\partial^2 E_p}{\partial x^2}\delta x^2 + \frac{1}{2}\frac{\partial^2 E_p}{\partial z^2}\delta z^2 + \frac{1}{2}\frac{\partial^2 E_p}{\partial y^2}\delta y^2 \tag{S6}$$

where E_p is given by eqn (5) in the main-text. In equilibrium, all the first order partial derivatives of the total potential energy are equal to zero,

$$\frac{\partial E_p}{\partial y} = \frac{\partial A(l)}{\partial y} - F^* = \frac{\partial A(l)}{\partial l}\frac{\partial l}{\partial y} - F^* = \frac{\partial A(l)}{\partial l}\frac{y}{l} - F^* = 0 \tag{S7}$$

At the equilibrium position $\vec{r}_0 = (0, y_0, z_0)$, $\alpha = 0$, $y = l\cos\theta$ and $F^* = F_\mathrm{tether}\cos\theta$ where F_tether is the tension along DNA, so we have

$$\frac{\partial A(l)}{\partial l} = F^*\frac{l}{y} = \frac{F^*}{\cos\theta} = F_\mathrm{tether} \tag{S8}$$

For $\hat{x}$ direction,

$$\frac{\partial E_\mathrm{p}}{\partial x} = \frac{\partial A(l)}{\partial l}\frac{x}{l} \tag{S9}$$

$$\frac{\partial^2 E_{\mathrm{p}}}{\partial x^2} = \frac{\partial A(l) 1}{\partial l \quad l} + \frac{\partial^2 A(l)}{\partial l^2} \left(\frac{x}{l}\right)^2 - \frac{\partial A(l) x^2}{\partial l \quad l^3} \tag{S10}$$

Around the equilibrium position $\vec{r}_0 = (0, y_0, z_0)$,

$$\frac{\partial^2 E_{\mathrm{p}}}{\partial x^2} \approx \frac{\partial A(l) 1}{\partial l \quad l} = \frac{F_{\mathrm{tether}}}{l} \tag{S11}$$

Thus, the average potential energy in $\hat{x}$ direction can be written as

$$\langle E_{\mathrm{p}} \rangle_x = \frac{1}{2} \frac{\partial^2 E_{\mathrm{p}}}{\partial x^2} \langle \delta x^2 \rangle = \frac{1}{2} \frac{F_{\mathrm{tether}}}{l} \langle \delta x^2 \rangle \tag{S12}$$

Using the equipartition theorem,[8]

$$\frac{1}{2} \frac{F_{\mathrm{tether}}}{l} \langle \delta x^2 \rangle = \frac{1}{2} k_{\mathrm{B}} T \tag{S13}$$

Consequently,

$$F_{\mathrm{tether}} = \frac{k_{\mathrm{B}} T l}{\langle \delta x^2 \rangle} \tag{S14}$$

Since the rotation fluctuation of the tethered bead in $\hat{x}$ direction around $\hat{z}$ axis is unconstrained, the fluctuation of the tethered bead in $\hat{x}$ direction can be considered as a pendulum with an equivalent length of $(l + r)$, where r is the radius of the tethered bead.[7, 9, 10]

Finally, F_{tether} and F^* can be written as,

$$F_{\mathrm{tether}} = \frac{k_{\mathrm{B}} T (l + r)}{\langle \delta x_{\mathrm{bead}}^2 \rangle} \tag{S15}$$

$$F^* = F_{\mathrm{tether}} \cos\theta = \frac{k_{\mathrm{B}} T (l + r) \cos\theta}{\langle \delta x_{\mathrm{bead}}^2 \rangle} = \frac{k_B T y_{\mathrm{bead}}}{\langle \delta x_{\mathrm{bead}}^2 \rangle} \tag{S16}$$

where $\langle \delta x_{\text{bead}}^2 \rangle$ is the variance of the tethered bead excursions in the $\hat{x}$ direction, and y_{bead} is the distance from the center of the tethered bead to the anchoring point in the $\hat{y}$ direction. In our calibration experiments, we use eqn (S16) to measure F^* as a function of flow rate V to work out the linear conversion factor k.

4.2 Theoretical caliculation of the hydrodynamic drag on DNA

According to the eqn (4) and eqn (6) in the main-text, the equivalent hydrodynamic drag on DNA, F_{drag}^*, is given by

$$F_{\text{drag}}^* = \frac{2}{3} F_{\text{drag}} = \frac{2}{3} \xi_0 \dot{\gamma} \frac{N+1}{2} z \tag{S17}$$

where ξ_0 is the friction coefficient for each bead, $\dot{\gamma}$ is the shear rate, N is the number of the base pairs, z is the height of one end of DNA (*i.e.*, point "O" as Fig. 1B shows) to the surface and F_{drag}^* is along the flow direction. Meiners *et al.* have measured the friction coefficient for λ-DNA (contour length L_0 = 16.4 μm or 48.5 kbp) with optical tweezers, showing that $\xi_{\lambda\text{-DNA, }//}$ = 7.6 × 10^{-9} N s m^{-1} in the longitudinal direction.[11] Because the friction coefficient of DNA is proportional to its contour length, based on their result, we can estimate the friction coefficient for one base pair DNA, ξ_0, to be ~ 1.567 × 10^{-13} N s m^{-1}. The shear rate $\dot{\gamma}$ can be calculated by the velocity distribution as shown in Section 3 in this Supplementary Information. The height of the end of DNA (point "O"), *i.e.*, z, can be determined by eqn (11) to eqn (16) in the main-text, given $z = l \cos\theta$. After all the parameters have been determined, F_{drag}^* can then be calculated. Fig. S8 shows the calculated F_{drag}^* as a function of F^* for the traces shown in Fig. 5. Finally, the total equivalent stretching force on DNA (which is along DNA direction and equal to the tension in DNA) can also be obtained by

$$F_{\text{tether}} = \frac{F_{\text{flow}} + F_{\text{drag}}^*}{\cos\theta} = F_{\text{bead}} + \frac{2F_{\text{drag}}}{3\cos\theta} \tag{S18}$$

where $F_{\text{bead}} = \frac{F_{\text{flow}}}{\cos\theta}$ is the force for DNA pulling the bead.

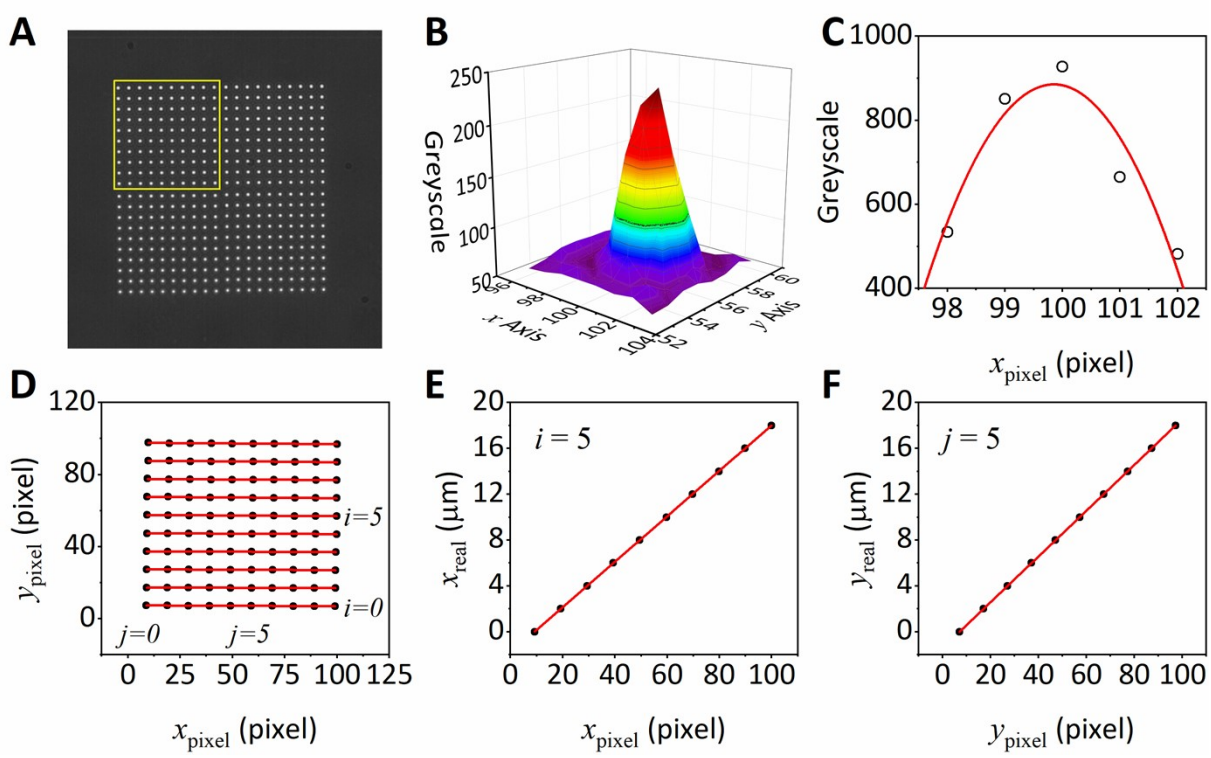

Fig. S1. The calibration of the pixel-distance relationship. (A) A picture of fabricated "nano-ruler" which is essentially an array of nano-holes. The diameter of each hole is ~160 nm and the spacing between the adjacent nano-holes is 2 μm. (B) The 2D distribution of the greyscale intensity of one nano-hole. (C) The accumulated greyscale intensity profile along $\hat{x}$. (D) The determined center positions (in pixel) of the 10×10 nano-holes selected by the yellow frame in (A). The red lines represent the linear fitting to the center positions of nano-holes of each row. The slope gives the tilt angle θ_i for the i^{th} row. (E) The x coordinate of the center position in pixel (x_{pixel}) *versus* its corresponding real-space position in μm (x_{real}). Red line is a linear fit with the slope k_i representing the x conversion factor for the i^{th} row (here i = 5). (F) Determination of the y conversion factor for the j^{th} column (here j = 5) using the same way as that for x in (E). Finally, we average all the k_i (for i=0 to 9) to obtain the x conversion factor which is 199.06 nm pixel^{-1}. Similarly, we can also obtain the y conversion factor which is 199.63 nm pixel^{-1}.

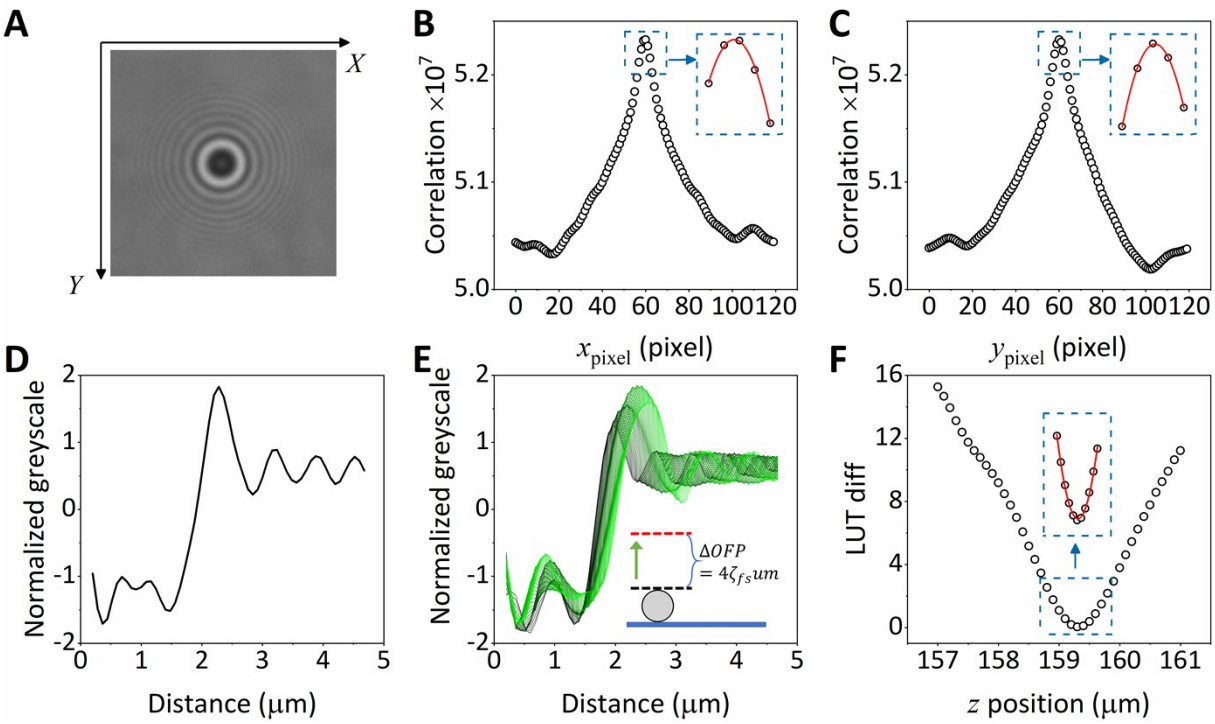

Fig. S2. Image analysis algorithm for real-time bead tracking. (A) A typical diffraction pattern of one M280 bead (r = 1400 nm) within the ROI (120 pixels × 120 pixels). (B) and (C) The correlation results for x and y coordinates after performing Fast Fourier Transform algorithm.[2-5] x_{center} and y_{center} are obtained by a 5-point quadratic fit (red line) around the maximum in the correlation signal, respectively. (D) The radial profile of the bead diffraction pattern constructed in a polar coordinate in which the bead center obtained in (B) and (C) is set as the origin. To correct for the fluctuations in the illumination light, the radial profile is normalized by subtracting its mean intensity and then dividing by the standard deviation of the intensity. (E) A typical Look-Up-Table used for determination of the bead's z position consists of a group of normalized radial profiles of bead's diffraction pattern. Here, it shows an example about how to build a LUT. The objective is moved by a nano-piezo stage from z_0 to (z_0+4) μm with a step size of 100 nm, as indicated in the cartoon. However, the objective focal plane only moves 4ζ_{fs} μm from the black dash line to the red. Here ζ_{fs} is the focal shift (~ 0.88). During the movement of objective, the bead's radial profile changes from the deep green curve to the light green curve. These radial profiles thus form the LUT. (F) The square of the differences between the measured bead's radial profile and all the radial profiles in LUT versus z position (focal shift not corrected yet). The final z position of the bead is obtained as the minimum in a ten-point quadratic fitting (red line) multiplied by ζ_{fs}.

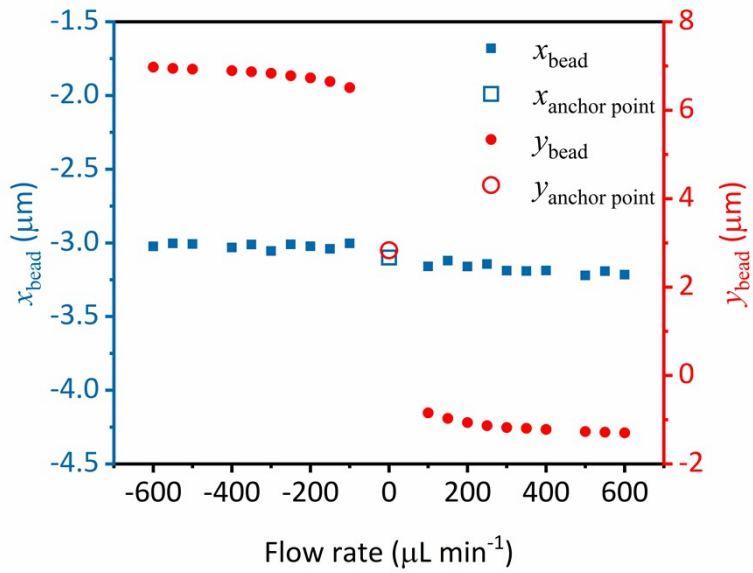

Fig. S3. Determination of the anchoring point of DNA. A pair of flows with the same rate but in opposite directions (the positive value of flow rate means withdrawing the buffer and the negative value means infusion) were used to stretch DNA. The bead position was recorded at the same time. For each flow step, the average position of the bead center is shown as blue solid square for x_{bead} and red solid circle for y_{bead}. Finally, we calculate the mean of the x_{bead} and y_{bead} from all pairs of flows to determine the final position of the anchoring point (i.e., $x_{anchor\ point}$ = -3099 ± 16 nm, mean ± S.D., blue open square and $y_{anchor\ point}$ = 2834 ± 5 nm, mean ± S.D., red open circle).

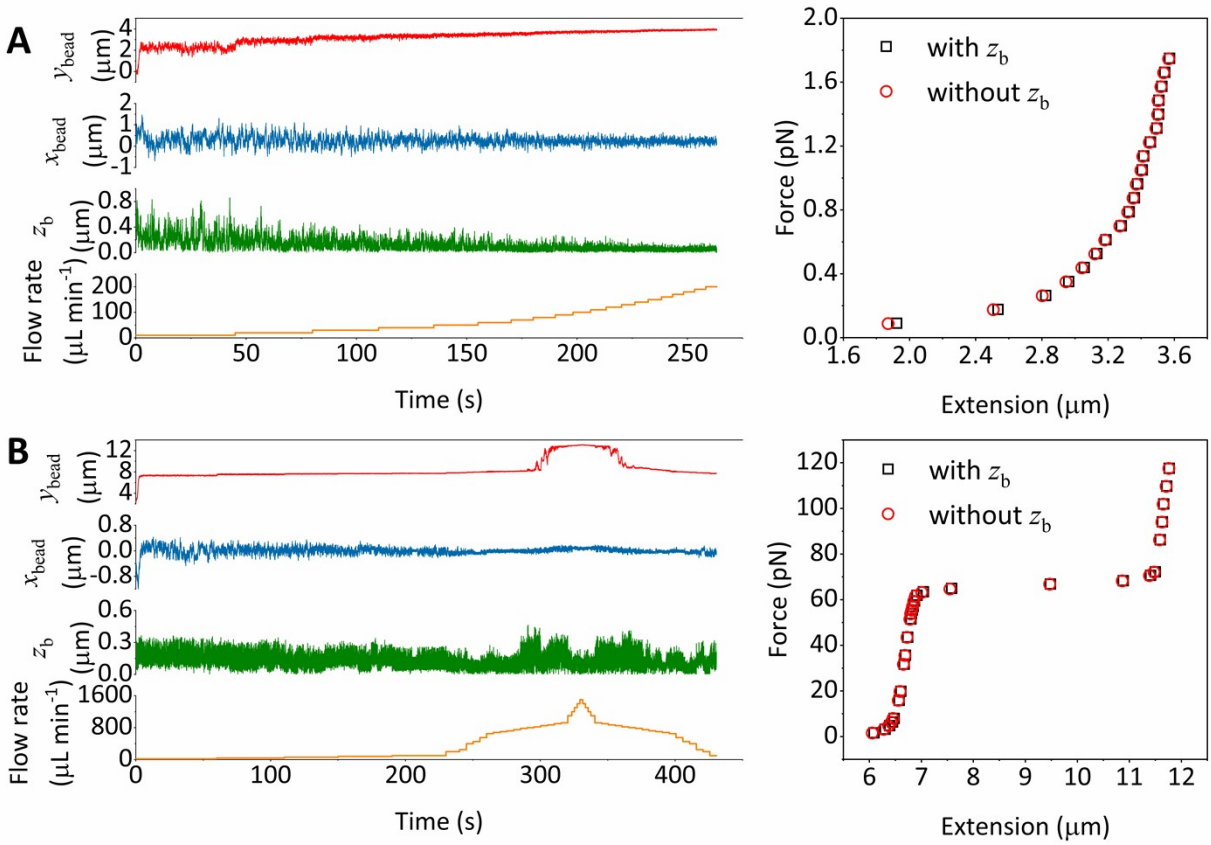

Fig. S4. Examples of measured raw trace and force-extension curves in the DNA-stretching experiment with (A) 800 nm polystyrene beads; (B) 2.8 μm M280 beads. Here, z_b signal represents the distance from the bead's bottom to the surface of coverslip. Notice that in (B) the DNA started to be overstretched at t ~300 s. Also, the measured force-extension curves with and without taking z_b signal into consideration are almost identical for DNA-stretching experiment with both 800 nm polystyrene beads and 2.8 μm M280 beads.

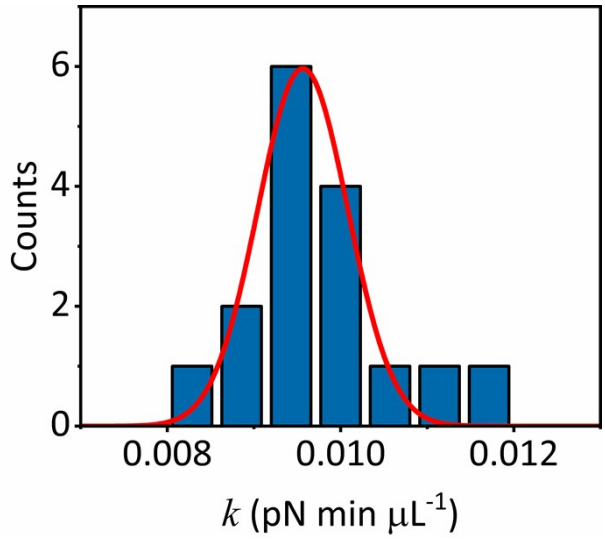

Fig. S5. The distribution of the calibrated k from 16 traces in Fig. 2 in DNA stretching experiment with 800 nm polystyrene bead. The final mean conversion factor is k = 0.0096 ± 0.0005 pN min μL^{-1} (mean ± S.D.) from the Gaussian fitting (the red line).

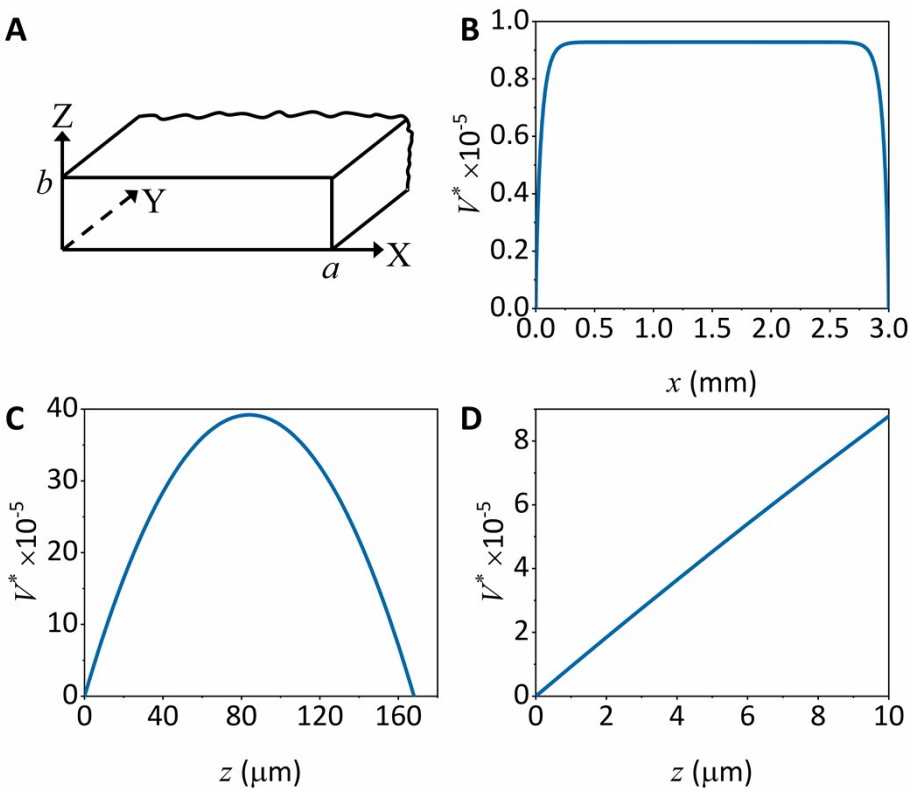

Fig. S6 Calculation of velocity distribution of the flow in the chamber. (A) The schematic of the flow-cell chamber used in the calculation. Here, a = 3 mm and b = 168 μm. (B) The calculated dimensionless velocity profile along $\hat{x}$ at z = 1 μm. (C) The calculated dimensionless velocity profile along $\hat{z}$ at x = 1500 μm. (D) Part of the velocity profile in (C). As can be seen, the profile is quite linear when z is close to the surface.

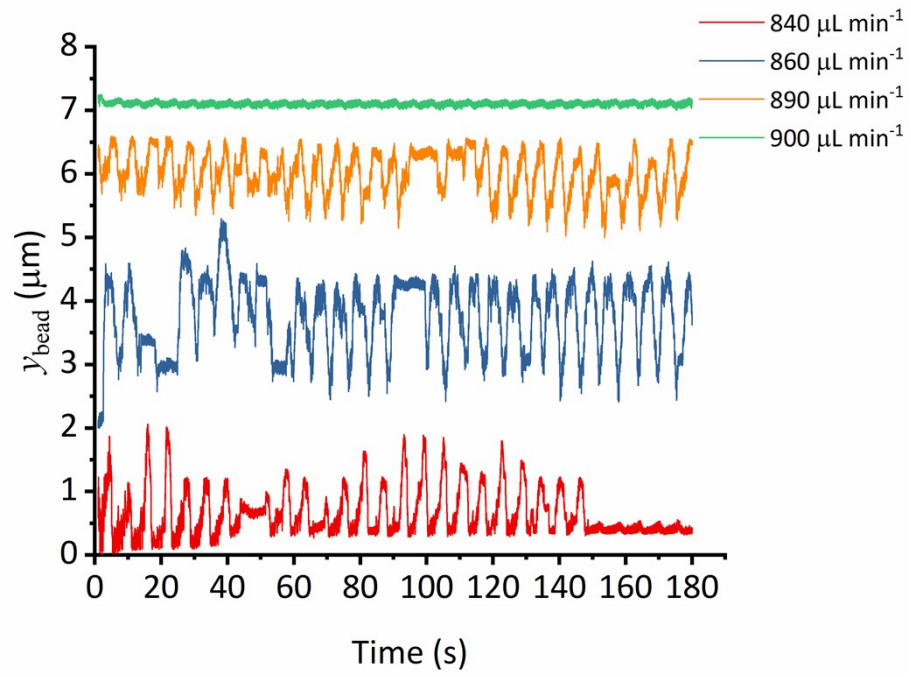

Fig. S7. The periodic noise introduced by the syringe pump which can be clearly seen as DNA starts to be overstretched. At this stage, DNA extension is highly sensitive to the force and hence the flow rate. A tether (contour length L_0 = 6800 nm) is under a constant flow or force for 3 min with different flow rate, 840, 860, 890, 900 µL min^{-1} from bottom to top, corresponding to 65.44, 66.99, 69.33, 70.11 pN, respectively (data were shifted for clarification). The oscillating noise during overstretching allowed us to roughly estimate the force stability of our system. According to the previous literature,[12] the change in extension (Δl) is about 0.65 times of the contour length and the change in force (ΔF) is about 5 pN from the beginning to the end of the DNA overstretching transition. Based on those parameter, for 860 µL min^{-1} data which exhibit largest extension oscillation (Δl is about 1.5 µm), we can calculate the corresponding force variation, $\Delta F = \frac{\Delta l \times 5}{0.65 \times L_0}$ = 1.70 pN. This result indicates that the force uncertainty or stability in our flow-cell system is ~ 2.6% due to the syringe pump, which is acceptable for most experiments. The noise is expected to be greatly diminished when replacing syringe pump with a gas pump. As a result, the force stability of the flow-cell system could be further improved in the future. Finally, it is worth mentioning that in the experiments, the average extension was used as the final extension at each flow rate.

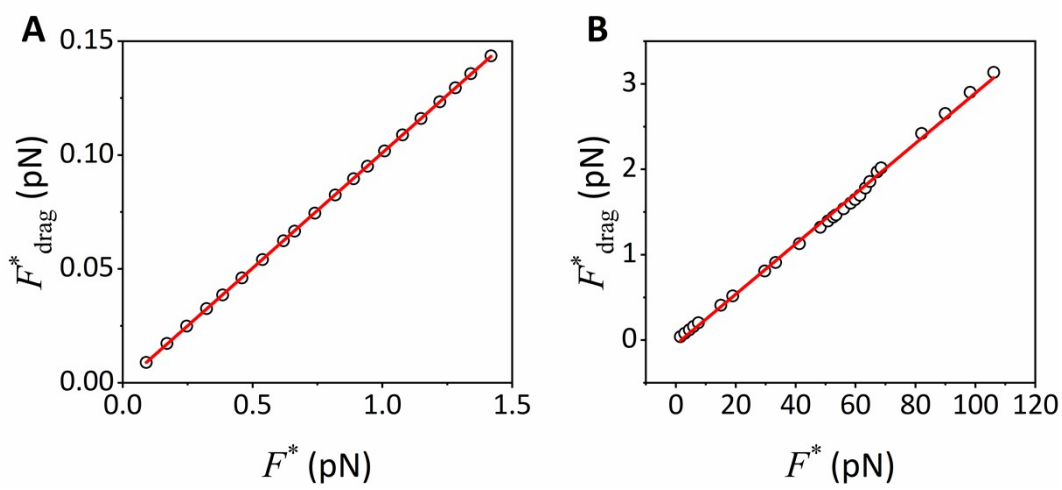

Fig. S8. The relationship between F^*_{drag} and F^* for DNA tethered with an 800 nm polystyrene bead (A) or a 2.8 μm M280 bead (B). F^*_{drag} is the equivalent hydrodynamic drag on DNA and F^* is the equivalent hydrodynamic drag on the bead-DNA system. The slope from the linear fitting (red line) gives the ratio of the F^*_{drag} to F^*, which is 0.10 for polystyrene bead (A) and 0.03 for M280 bead (B).

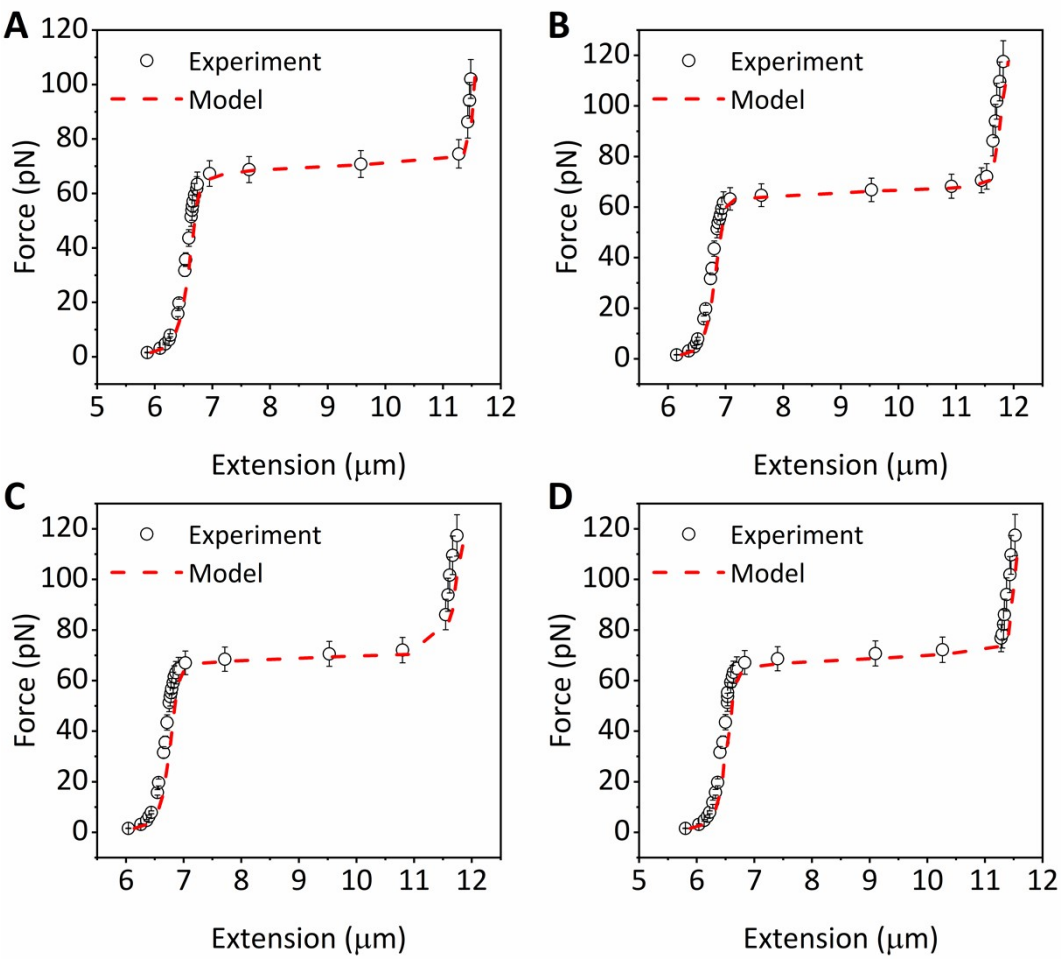

Fig. S9. More traces about the measured (black circle) and calculated force-extension curves (FECs) from theory (red dashed line) for DNA overstretching experiments with 2.8 μm M280 beads. (A)-(D) FECs from four different tethers. The theoretically calculated forces are ~2% lower than the experimental ones.

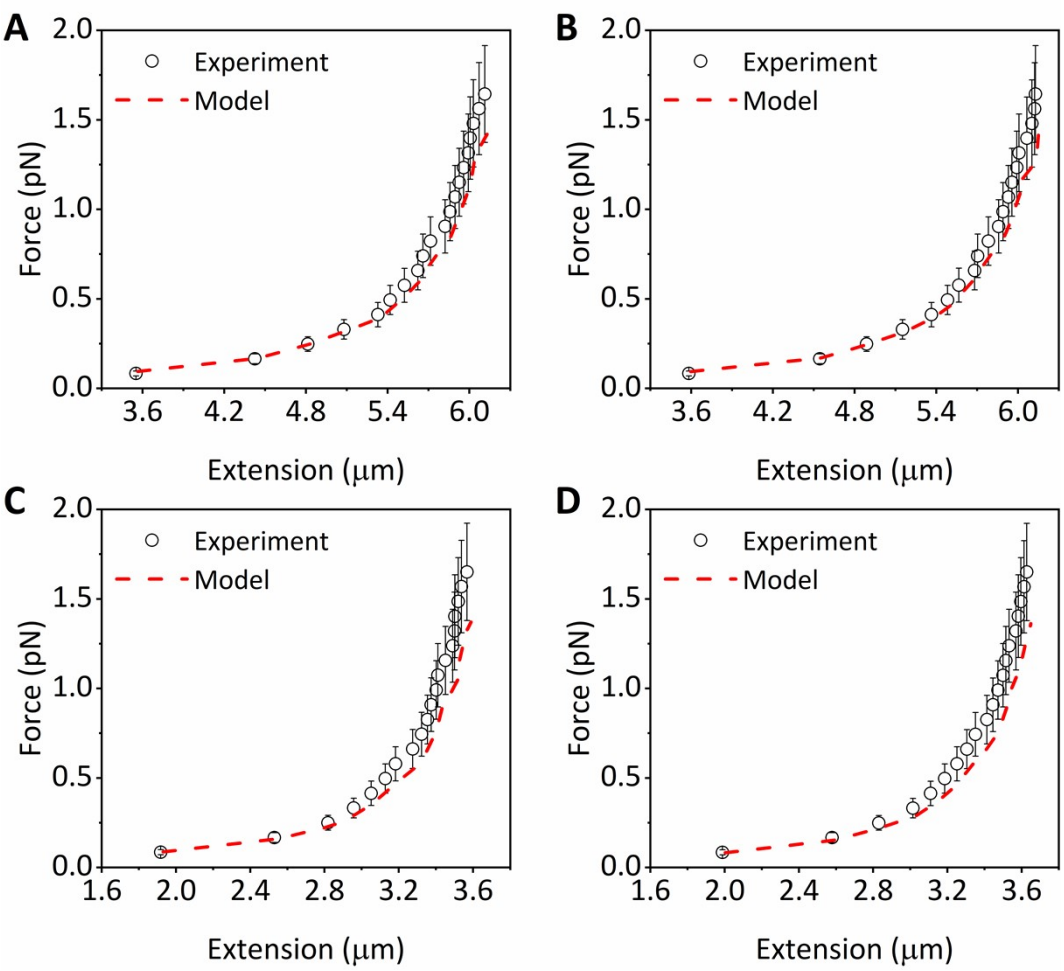

Fig. S10. More traces about the measured (black circle) and calculated force-extension curves from theory (red dashed line) for DNA stretching experiments with 800 nm polystyrene beads. (A)-(D) FECs from three different tethers. The theoretically calculated forces are ~12% lower than the experimental ones.

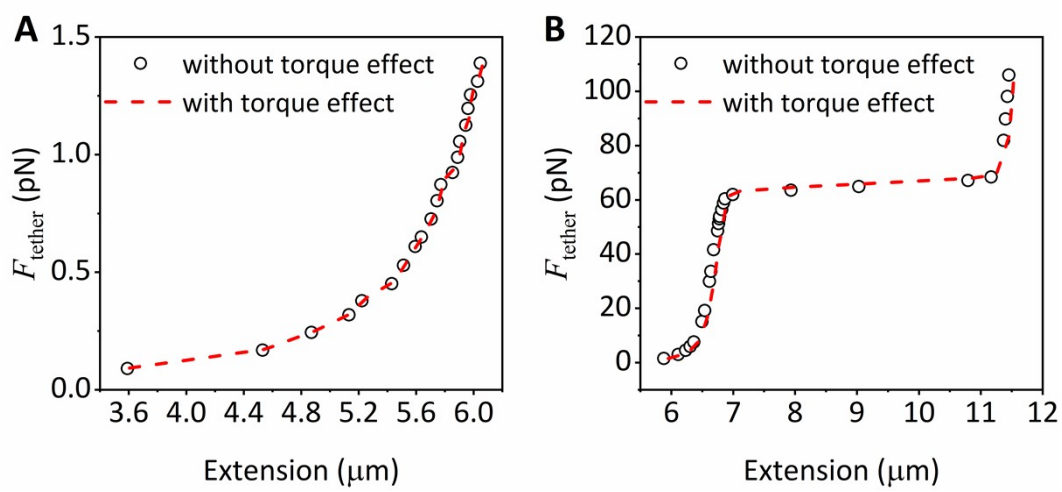

Fig. S11. The torque effect on the theoretical calculated FECs under different configurations. (A) DNA tethered with an 800 nm polysterence bead. (B) DNA tethered with a 2.8 μm M280 bead. It can be seen that, in both cases, the torque effect is insignificant and negligible.

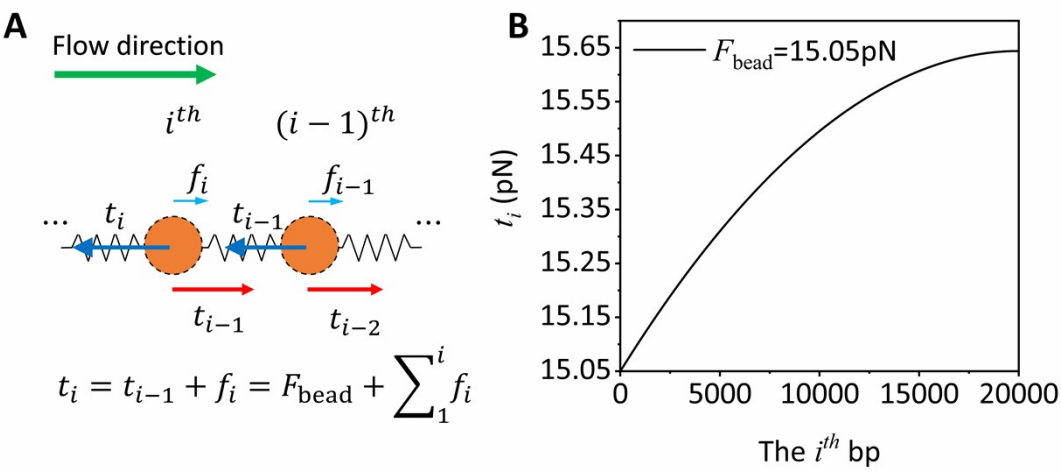

Fig. S12. The uneven tension in DNA caused by the hydrodynamic drag from the flow. (A) For the i^{th} bead, the tension t_i is in balance with the tension $t_{i\text{-}1}$ and the friction force f_i. Finally, $t_i = F_{\text{bead}} + \sum_1^i f_i$, where F_{bead} is the stretching force due to the tether bead. (B) The distribution of the tension along DNA when F_{bead} = 15.05 pN and using M280 beads. As can be seen, the tension along DNA only varies ~4%, which causes ~0.12% variation of the extesnion between the first bp and the last bp (*i.e.* the 1st bp and the 20000th bp) of DNA. When using 800 nm polystyrene beads at F_{bead} = 0.15 pN, this tension variation becomes ~ 17%, which however only causes ~6.0% variation of the extesnion between the first bp and the last bp of DNA. It also should be noticed that this variation of the extension will decrease as F_{bead} increaces while the variation of the tension along DNA is insensitive to F_{bead}. Therefore, the DNA extension of each unit in (A) can be approximated to be equal under our experimental configurations.

Table S1. The nomenclature of the forces used in this paper.

F_{flow}	the hydrodynamic force on the tethered bead, which is along the flow direction
F_{drag}	the hydrodynamic drag (*i.e.* the total friction force) on the DNA, which is along the flow direction
F^*_{drag}	the equivalent hydrodynamic drag on DNA, which is along the flow direction
F^*	the equivalent hydrodynamic force on the bead-DNA system, which is along the flow direction
F_{bead}	the force for DNA pulling the tethered bead, which is along the DNA direction
F_{tether}	the equivalent stretching force on DNA, or the equivalent tension in DNA, which is along the DNA direction

Supporting Reference:

1. M. Wu, W. Liu, J. Hu, Z. Zhong and J. Ma, *Opt. Express*, 2019, **27**, 19002.
2. M. T. van Loenhout, J. W. Kerssemakers, I. De Vlaminck and C. Dekker, *Biophys. J.*, 2012, **102**, 2362-2371.
3. J. P. Cnossen, D. Dulin and N. H. Dekker, *Rev. Sci. Instrum.*, 2014, **85**, 103712.
4. G. Sitters, D. Kamsma, G. Thalhammer, M. Ritsch-Marte, E. J. G. Peterman and G. J. L. Wuite, *Nat. Methods*, 2015, **12**, 47-50.
5. C. Gosse and V. Croquette, *Biophys. J.*, 2002, **82**, 3314-3329.
6. M. Spiga and G. L. Morino, *Int. Commun. Heat Mass Transfer*, 1994, **21**, 469-475.
7. A. J. W. te Velthuis, J. W. J. Kerssemakers, J. Lipfert and N. H. Dekker, *Biophys. J.*, 2010, **99**, 1292-1302.
8. T. R. Strick, J.-F. Allemand, D. Bensimon, A. Bensimon and V. Croquette, *Science*, 1996, **271**, 1835-1837.
9. H. Chen, H. Fu, X. Zhu, P. Cong, F. Nakamura and J. Yan, *Biophys. J.*, 2011, **100**, 517-523.
10. Y. Harada, O. Ohara, A. Takatsuki, H. Itoh, N. Shimamoto and K. Kinosita, *Nature*, 2001, **409**, 113-115.
11. J.-C. Meiners and S. Quake, *Phys. Rev. Lett.*, 2000, **84**, 5014-5017.
12. S. Cocco, J. Yan, J. F. Leger, D. Chatenay and J. F. Marko, *Phys. Rev. E*, 2004, **70**, 011910.